

Exact Results for the Orbital Angular Momentum of Magnons on Honeycomb Lattices

Randy S. Fishman,^{1,*} Lucas Lindsay,¹ and Satoshi Okamoto¹

¹*Materials Science and Technology Division, Oak Ridge National Laboratory, Oak Ridge, Tennessee 37831, USA*
(Dated: September 30, 2022)

We obtain exact results for the orbital angular momentum (OAM) of magnons at the high symmetry points of ferromagnetic (FM) and antiferromagnetic (AF) honeycomb lattices in the presence of Dzyaloshinskii-Moriya (DM) interactions. For the FM honeycomb lattice in the absence of DM interactions, the values of the OAM at the corners of the Brillouin zone (BZ) ($\mathbf{k}_1^* = (0, 2\sqrt{3}/9)2\pi/a$, $\mathbf{k}_2^* = (1/3, \sqrt{3}/9)2\pi/a, \dots$) are alternately $\pm 3\hbar/16$ for both magnon bands. The presence of DM interactions dramatically changes those values by breaking the degeneracy of the two magnon bands. The OAM values are alternately $3\hbar/8$ and 0 for the lower magnon band and $-3\hbar/8$ and 0 for the upper magnon band. For the AF honeycomb lattice, the values of the OAM at the corners of the BZ are $\mp(3\hbar/16)\kappa$ on one of the degenerate magnon bands and $\pm(3\hbar/8)(1 + \kappa/2)$ on the other, where κ measures the anisotropy and the result is independent of the DM interaction.

I. INTRODUCTION

The conversion of spin into orbital angular momentum and back has been of great interest since the early measurements of Einstein and deHass [1] and Barnett [2]. One recently posed question [3–6] is whether spin excitations, commonly called magnons, can have both spin and orbital angular momentum (OAM). While the magnon produced by a ferromagnet (FM) with moments up has spin $\mathcal{S} = -\hbar$, its OAM \mathcal{L} is not known. The observation of the OAM associated with magnons would have wide-ranging physical ramifications. Since the total angular momentum $\mathcal{J} = \mathcal{S} + \mathcal{L}$ is conserved [7, 8], magnons with \mathcal{S} parallel to \mathcal{L} and those with \mathcal{S} antiparallel to \mathcal{L} will behave differently under collisions and in external fields. Consequently, memory storage devices may be able to utilize the OAM of magnons in the developing field of magnonics [9]. It is likely that the magnon Hall [10–12] and Nernst [13] effects will sensitively depend on the OAM of the magnons. Another fascinating possibility is that magnons with OAM can be created and controlled by the interaction with photons [14] and phonons [15, 16] that also carry OAM.

In a recent paper [17], two of us demonstrated that the magnons of collinear magnets may exhibit OAM even for simple collinear magnets. Surprisingly, the OAM of magnons on FM and antiferromagnetic (AF) zig-zag and honeycomb lattices in two dimensions depends on the network of exchange interactions and not on spin-orbit (SO) coupling, as was proposed in Ref. [5]. Rather, we found that the confinement of magnons can generate an effective OAM by disrupting the locally symmetric environment at each lattice site. In that sense, our previous efforts followed earlier studies of the OAM of magnons in confined spherical [18–20] and cylindrical [21–23] geometries. At least formally, our results also reduced to the well-known expressions of Matsumoto and Murakami [3, 4] for the self-rotation of magnon packets in the case

of FM systems at low excitation energies.

Our previous work was based almost entirely on numerical simulations. In this paper, we obtain exact results for the OAM of magnons on FM and AF honeycomb lattices at the corners \mathbf{k}^* of the Brillouin zone (BZ) in reciprocal space (see Fig. 2) in the presence of Dzyaloshinski-Moriya (DM) interactions, which are induced by SO interactions. In addition to providing checks on our numerics, this work also provides deeper insight into the profound and unexpected effects of the DM interaction on the OAM of honeycomb lattices. For a FM honeycomb lattice, we find that DM interactions can dramatically change the amplitude of the OAM near the BZ corners.

Section II summarizes the OAM formalism for the magnons of FM and AF honeycomb lattices. Section III presents our results for the FM honeycomb lattice in the absence of DM interactions. We then add DM interactions in Section IV. Section V treats the AF honeycomb lattice. Finally, Section VI contains a conclusion.

II. OAM FORMALISM

As sketched in Fig. 1, honeycombs are non-Bravais lattices with two unique sites 1 and 2. The total magnetization \mathbf{M}_i at site i can be written in terms of the dynamical magnetization $\boldsymbol{\mu}_i$ as

$$\mathbf{M}_i = \boldsymbol{\mu}_i + \mathbf{n}_i \sqrt{M_0^2 - \mu_i^2}, \quad (1)$$

where the static magnetization $\mathbf{M}_{0i} = 2\mu_B S \mathbf{n}_i$ lies along $\mathbf{n}_i = \pm \mathbf{z}$ and $\boldsymbol{\mu}_i \cdot \mathbf{n}_i = 0$. The “pseudo-momentum” \mathbf{p}_i is derived [17] from the energy-momentum tensor $T_{\alpha\beta}$ [24] for a model spin Lagrangian

$$L = \frac{1}{4\mu_B M_0} \sum_{i=1}^N (\dot{\boldsymbol{\mu}}_i \times \mathbf{n}_i) \cdot \boldsymbol{\mu}_i - H_2, \quad (2)$$

* corresponding author: fishmanrs@ornl.gov

where H_2 is obtained by expanding the Hamiltonian

$$H = - \sum_{i=1}^N J_{\alpha\beta} M_{i\alpha} M_{i+1,\beta} - \sum_{i=1}^N \mathbf{M}_i \cdot \mathbf{h}_i - \frac{K}{4\mu_B^2} \sum_{i=1}^N M_{iz}^2 - \frac{1}{8\pi} \sum_{i=1}^N h_i^2, \quad (3)$$

to second order in μ_i . Here, the exchange $J_{\alpha\beta}$ includes possible antisymmetric terms like the DM interaction, the magnetic dipole field \mathbf{h}_i satisfies $\nabla \times \mathbf{h}_i = 0$ and $\nabla \cdot \mathbf{h}_i = -4\pi \nabla \cdot \mathbf{M}_i$, and K is the easy-axis anisotropy along \mathbf{z} . It is straightforward to show [7, 8] that the Hamiltonian equations of motion for μ_i can also be obtained from the Euler-Lagrange equations for L . Consequently,

$$p_{i\alpha} = - \frac{\partial \mu_i}{\partial x_\alpha} \cdot \frac{\partial L}{\partial \mu_i} = - \frac{1}{4\mu_B M_0} (\mathbf{n}_i \times \mu_i) \cdot \frac{\partial \mu_i}{\partial x_\alpha}. \quad (4)$$

is the momentum at site i

Within linear spin-wave theory, the $1/S$ quantization conditions

$$\mu_i^+ = \mu_{ix} n_{iz} + i\mu_{iy} = 2\mu_B \sqrt{2S\hbar} a_i, \quad (5)$$

$$\mu_i^- = \mu_{ix} n_{iz} - i\mu_{iy} = 2\mu_B \sqrt{2S\hbar} a_i^\dagger \quad (6)$$

are formulated in terms of local Boson operators a_i and a_i^\dagger that satisfy the real-space commutation relations $[a_i, a_j^\dagger] = \delta_{ij}$ and $[a_i, a_j] = 0$. Transforming to momentum space with r and s denoting positions within the magnetic unit cell, we define Boson operators $a_{\mathbf{k}}^{(r)}$ and $a_{\mathbf{k}}^{(r)\dagger}$ satisfying the commutation relations $[a_{\mathbf{k}}^{(r)}, a_{\mathbf{k}'}^{(s)\dagger}] = \delta_{rs} \delta_{\mathbf{k},\mathbf{k}'}$ and $[a_{\mathbf{k}}^{(r)}, a_{\mathbf{k}'}^{(s)}] = 0$. We may then write the OAM along \mathbf{z} as [17]

$$\begin{aligned} \mathcal{L}_z &= \sum_{i=1}^N (\mathbf{R}_i \times \mathbf{p}_i) \cdot \mathbf{z} \\ &= \frac{1}{8\mu_B M_0} \sum_{i=1}^N \left\{ \mu_i^+ \hat{l}_{zi} \mu_i^- - \mu_i^- \hat{l}_{zi} \mu_i^+ \right\} \\ &= \frac{\hbar}{2} \sum_{r=1}^2 \sum_{\mathbf{k}} \left\{ a_{\mathbf{k}}^{(r)} \hat{l}_{z\mathbf{k}} a_{\mathbf{k}}^{(r)\dagger} - a_{\mathbf{k}}^{(r)\dagger} \hat{l}_{z\mathbf{k}} a_{\mathbf{k}}^{(r)} \right\}, \end{aligned} \quad (7)$$

where

$$\hat{l}_{zi} = -i \left(x_i \frac{\partial}{\partial y_i} - y_i \frac{\partial}{\partial x_i} \right), \quad (8)$$

$$\hat{l}_{z\mathbf{k}} = -i \left(k_x \frac{\partial}{\partial k_y} - k_y \frac{\partial}{\partial k_x} \right) \quad (9)$$

are the OAM operators in real and momentum space.

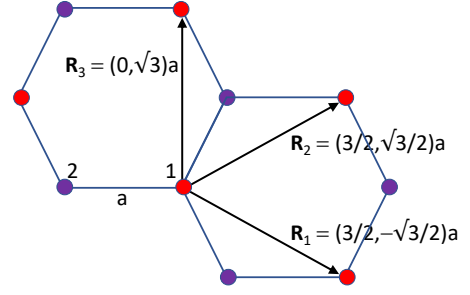


FIG. 1. A honeycomb lattice with unique sites 1 and 2 and the translation vectors $\mathbf{R}_1 = (3/2, -\sqrt{3}/2)a$, $\mathbf{R}_2 = (3/2, \sqrt{3}/2)a$, and $\mathbf{R}_3 = (0, \sqrt{3})a$ coupling neighboring sites 1.

Converting $a_{\mathbf{k}}^{(r)}$ and $a_{\mathbf{k}}^{(r)\dagger}$ to the Boson operators $b_{\mathbf{k}}^{(n)}$ and $b_{\mathbf{k}}^{(n)\dagger}$ that diagonalize the Hamiltonian in terms of the eigenmodes $|\mathbf{k}, n\rangle = b_{\mathbf{k}}^{(n)\dagger} |0\rangle$ with frequencies $\omega_n(\mathbf{k})$ ($n = 1, 2$), we define [25]

$$a_{\mathbf{k}}^{(r)} = \sum_{n=1}^2 \left\{ X^{-1}(\mathbf{k})_{rn} b_{\mathbf{k}}^{(n)} + X^{-1}(\mathbf{k})_{r,n+2} b_{-\mathbf{k}}^{(n)\dagger} \right\}, \quad (10)$$

$$a_{-\mathbf{k}}^{(r)\dagger} = \sum_{n=1}^2 \left\{ X^{-1}(\mathbf{k})_{r+2,n} b_{\mathbf{k}}^{(n)} + X^{-1}(\mathbf{k})_{r+2,n+2} b_{-\mathbf{k}}^{(n)\dagger} \right\}.$$

The zero-temperature expectation value of \mathcal{L}_z in eigenmode n is then given by

$$\begin{aligned} \mathcal{L}_{zn}(\mathbf{k}) &= \langle \mathbf{k}, n | \mathcal{L}_z | \mathbf{k}, n \rangle \\ &= \frac{\hbar}{2} \sum_{r=1}^2 \left\{ X^{-1}(\mathbf{k})_{rn} \hat{l}_{z\mathbf{k}} X^{-1}(\mathbf{k})_{rn}^* \right. \\ &\quad \left. - X^{-1}(\mathbf{k})_{r+2,n} \hat{l}_{z\mathbf{k}} X^{-1}(\mathbf{k})_{r+2,n}^* \right\}. \end{aligned} \quad (11)$$

For collinear spin states *without* symmetry-breaking DM interactions, $\underline{X}^{-1}(-\mathbf{k}) = \underline{X}^{-1}(\mathbf{k})^*$ so that $\mathcal{L}_{zn}(\mathbf{k}) = -\mathcal{L}_{zn}(-\mathbf{k})$ is an odd function of \mathbf{k} . The 4×4 -dimensional matrix $\underline{X}(\mathbf{k})$ will feature prominently in our subsequent discussion.

Due to the linear terms k_x and k_y in the OAM operator $\hat{l}_{z\mathbf{k}}$ of Eq. (9), the resulting $\mathcal{L}_{zn}(\mathbf{k})$ is *not* a periodic function of \mathbf{k} in reciprocal space. This shortcoming arises because the “pseudo-momentum” \mathbf{p}_i in $\mathcal{L}_z = \sum_i (\mathbf{R}_i \times \mathbf{p}_i) \cdot \mathbf{z}$ contains the derivatives $\partial/\partial x_i$ and $\partial/\partial y_i$ from Eq. (4) that enter the real-space OAM operator \hat{l}_{zi} of Eq. (8). On a discrete lattice, those continuous derivatives should be replaced by finite differences.

The finite difference of a discrete function $f(\mathbf{r})$ produced by the translation vector \mathbf{R}_l is

$$\delta_l f(\mathbf{r}) = \frac{1}{2|\mathbf{R}_l|} \left\{ f(\mathbf{r} + \mathbf{R}_l) - f(\mathbf{r} - \mathbf{R}_l) \right\}. \quad (12)$$

Transforming the continuous derivative $\partial f(\mathbf{r})/\partial r_\alpha$ by

summing over distinct translation vectors \mathbf{R}_l , we obtain

$$\begin{aligned}\Delta_\alpha f(\mathbf{r}) &= \sum_l \frac{R_{l\alpha}}{|\mathbf{R}_l|} \delta_l f(\mathbf{r}) \\ &= \sum_l \frac{R_{l\alpha}}{2|\mathbf{R}_l|^2} \left\{ f(\mathbf{r} + \mathbf{R}_l) - f(\mathbf{r} - \mathbf{R}_l) \right\},\end{aligned}\quad (13)$$

where $R_{l\alpha}$ is the projection of \mathbf{R}_l along the α axis. Note that $\Delta_\alpha f(\mathbf{r}) \rightarrow \partial f(\mathbf{r})/\partial r_\alpha$ when the lattice translation vectors \mathbf{R}_l are orthogonal and their sizes vanish.

The Fourier transform of a magnon annihilation operator contains the factor $\exp(i\mathbf{k}\cdot\mathbf{r})$, which has the discrete difference

$$\begin{aligned}\Delta_\alpha \exp(i\mathbf{k}\cdot\mathbf{r}) &= i \exp(i\mathbf{k}\cdot\mathbf{r}) \sum_l \frac{R_{l\alpha}}{|\mathbf{R}_l|^2} \sin(\mathbf{k}\cdot\mathbf{R}_l) \\ &= i\bar{k}_\alpha \exp(i\mathbf{k}\cdot\mathbf{r})\end{aligned}\quad (14)$$

with periodic function

$$\bar{k}_\alpha = \sum_l \frac{R_{l\alpha}}{|\mathbf{R}_l|^2} \sin(\mathbf{k}\cdot\mathbf{R}_l).\quad (15)$$

For the honeycomb lattice in Fig. 1, summing over the three translation vectors \mathbf{R}_l that couple site 1 to three neighboring sites of type 1 produces

$$\begin{aligned}\bar{k}_x a &= \sin(3k_x a/2) \cos(\sqrt{3}k_y a/2), \\ \bar{k}_y a &= \frac{1}{\sqrt{3}} \left\{ \sin(\sqrt{3}k_y a/2) \cos(3k_x a/2) \right. \\ &\quad \left. + \sin(\sqrt{3}k_y a) \right\}.\end{aligned}\quad (16)$$

In the limit of small k_x and k_y , $\bar{k}_x \rightarrow 3k_x/2$ and $\bar{k}_y \rightarrow 3k_y/2$.

The revised OAM operator in momentum space is then given by

$$\hat{l}_{z\mathbf{k}} = -i \left(\bar{k}_x \frac{\partial}{\partial k_y} - \bar{k}_y \frac{\partial}{\partial k_x} \right).\quad (17)$$

In the limit $a \rightarrow 0$, there is no need to replace the *momentum space* derivatives $\partial/\partial k_x$ and $\partial/\partial k_y$ by finite differences. Using the periodic functions \bar{k}_x and \bar{k}_y instead of k_x and k_y imposes a natural bound on the OAM. As seen below, this replacement has important consequences for the OAM at the high-symmetry points of the honeycomb lattice.

For a FM state in the limit of small energies and momenta, our results for the OAM (Eqs. (11) and (17)) reduce to the expression of Matsumoto and Murakami [3, 4], which was parameterized in terms of a density-of-states and an effective mass. Since we are interested in the OAM of both FM and AF magnons throughout the BZ, we prefer to work with the more general expressions given above.

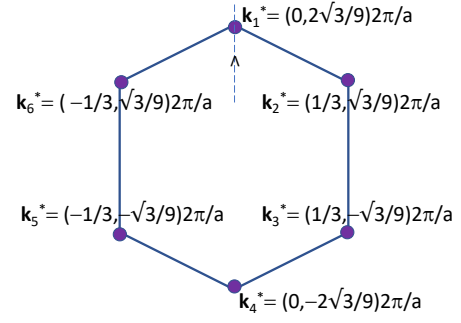


FIG. 2. The reciprocal-space hexagon of the honeycomb lattice showing the high-symmetry points \mathbf{k}^* . Direction of approach to \mathbf{k}_1^* used to evaluate the OAM is drawn as an arrow.

III. FM HONEYCOMB WITH $D = 0$

We first consider the FM honeycomb lattice shown in Fig. 3(a) with spins up, exchange coupling $J > 0$, and no DM interaction. The Hamiltonian is then

$$H = -J \sum_{\langle i,j \rangle} \mathbf{S}_i \cdot \mathbf{S}_j,\quad (18)$$

where the sum runs over all nearest neighbors of the honeycomb lattice. Second order in the vector operator $\mathbf{v}_{\mathbf{k}} = (a_{\mathbf{k}}^{(1)}, a_{\mathbf{k}}^{(2)}, a_{-\mathbf{k}}^{(1)\dagger}, a_{-\mathbf{k}}^{(2)\dagger})$, the Hamiltonian $H_2 = \sum_{\mathbf{k}} \mathbf{v}_{\mathbf{k}}^\dagger \cdot \underline{L}(\mathbf{k}) \cdot \mathbf{v}_{\mathbf{k}}$ is given by

$$\underline{L}(\mathbf{k}) = \frac{3JS}{2} \begin{pmatrix} 1 & -\Gamma_{\mathbf{k}}^* & 0 & 0 \\ -\Gamma_{\mathbf{k}} & 1 & 0 & 0 \\ 0 & 0 & 1 & -\Gamma_{\mathbf{k}}^* \\ 0 & 0 & -\Gamma_{\mathbf{k}} & 1 \end{pmatrix},\quad (19)$$

where

$$\begin{aligned}\Gamma_{\mathbf{k}} &= \frac{1}{3} \left\{ e^{ik_x a} + e^{-i(k_x + \sqrt{3}k_y)a/2} \right. \\ &\quad \left. + e^{-i(k_x - \sqrt{3}k_y)a/2} \right\}.\end{aligned}\quad (20)$$

The magnon dynamics is determined by diagonalizing $\underline{L} \cdot \underline{N}$, where

$$\underline{N} = \begin{pmatrix} \underline{I} & 0 \\ 0 & -\underline{I} \end{pmatrix}\quad (21)$$

and \underline{I} is the two-dimensional identity matrix. Using the relation $\underline{N} \cdot \underline{X}^\dagger(\mathbf{k}) \cdot \underline{N} = \underline{X}^{-1}(\mathbf{k})$ to normalize the eigenvectors [25] $\underline{X}^{-1}(\mathbf{k})_{rn}$, we find

$$\underline{X}^{-1}(\mathbf{k}) = \frac{1}{\sqrt{2}\Gamma_{\mathbf{k}}^*} \begin{pmatrix} -\Gamma_{\mathbf{k}}^* & \Gamma_{\mathbf{k}}^* & 0 & 0 \\ |\Gamma_{\mathbf{k}}| & |\Gamma_{\mathbf{k}}| & 0 & 0 \\ 0 & 0 & -\Gamma_{\mathbf{k}}^* & \Gamma_{\mathbf{k}}^* \\ 0 & 0 & |\Gamma_{\mathbf{k}}| & |\Gamma_{\mathbf{k}}| \end{pmatrix}.\quad (22)$$

It is then simple to show that

$$\mathcal{L}_{zn}(\mathbf{k}) = \frac{\hbar}{4} \frac{\Gamma_{\mathbf{k}}}{|\Gamma_{\mathbf{k}}|} \hat{l}_{z\mathbf{k}} \frac{\Gamma_{\mathbf{k}}^*}{|\Gamma_{\mathbf{k}}|}\quad (23)$$

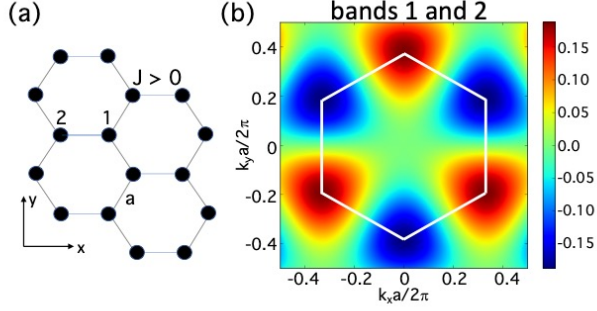


FIG. 3. (a) A honeycomb lattice with FM exchange $J > 0$. (b) The OAM for the bands 1 and 2 versus \mathbf{k} .

is the same for magnon bands $n = 1$ and 2 with frequencies $\omega_{1,2}(\mathbf{k}) = 3JS(1 \pm |\Gamma_{\mathbf{k}}|)$ (1 for +, 2 for -).

The upper and lower mode frequencies $\omega_1(\mathbf{k})$ and $\omega_2(\mathbf{k})$ cross at wavevectors $\mathbf{k}_1^* = (0, 2\sqrt{3}/9)2\pi/a$, $\mathbf{k}_2^* = (1/3, \sqrt{3}/9)2\pi/a$, and symmetry-related points \mathbf{k}^* at the corners of the BZ where $\Gamma_{\mathbf{k}^*} = 0$. As seen in Fig. 3(b), $\mathcal{L}_{zn}(\mathbf{k}^*)$ has alternating values of $\sim \pm 0.185\hbar$ at these crossing points with the positive value $\sim 0.185\hbar$ at \mathbf{k}_1^* ,

To analytically evaluate the OAM at \mathbf{k}_1^* , we construct the unit vector ($\mathbf{k} \neq \mathbf{k}_1^*$)

$$\hat{u}(\mathbf{k}) \equiv \frac{\Gamma_{\mathbf{k}}}{|\Gamma_{\mathbf{k}}|} = \frac{e^{ik_x a/4}}{C(\mathbf{k})} \left\{ A_+(\mathbf{k}) \cos(3k_x a/4) + iA_-(\mathbf{k}) \sin(3k_x a/4) \right\}, \quad (24)$$

where $A_{\pm}(\mathbf{k}) = 1 \pm 2 \cos(\sqrt{3}k_y a/2)$ and

$$C(\mathbf{k}) = \left\{ 1 + 4 \cos^2(\sqrt{3}k_y a/2) + 4 \cos(\sqrt{3}k_y a/2) \cos(3k_x a/2) \right\}^{1/2}. \quad (25)$$

Because

$$\mathcal{L}_{zn}(\mathbf{k}) = -\frac{i\hbar}{4} \hat{u}(\mathbf{k}) \left(\bar{k}_x \frac{\partial \hat{u}(\mathbf{k})^*}{\partial k_y} - \bar{k}_y \frac{\partial \hat{u}(\mathbf{k})^*}{\partial k_x} \right) \quad (26)$$

is singular at \mathbf{k}_1^* , we calculate the OAM at fixed $k_{1x}^* = 0$ while $k_{1y}^* = (2\sqrt{3}/9)2\pi/a$ is approached from below, as sketched in Fig. 2. (Of course, the OAM can also be evaluated by approaching \mathbf{k}_1^* from above or from any other direction.) We shall then evaluate the OAM at other BZ corners \mathbf{k}_m^* by applying a rotation operator.

When $k_x = 0$ but $k_y < (2\sqrt{3}/9)2\pi/a$, $\Gamma_{\mathbf{k}} = 1 + 2 \cos(\sqrt{3}k_y a/2)$ and $\hat{u}(\mathbf{k}) = 1$. It is then straightforward to show that

$$\lim_{k_x \rightarrow 0} \frac{\partial \hat{u}(\mathbf{k})^*}{\partial k_x} = -\frac{3ia}{2} \frac{1}{1 + 2 \cos(\sqrt{3}k_y a/2)}. \quad (27)$$

Since $\bar{k}_x \partial \hat{u}(\mathbf{k}) / \partial k_y$ vanishes as $k_x \rightarrow 0$, we obtain

$$\begin{aligned} \mathcal{L}_{zn}(\mathbf{k}_1^*) &= \frac{i\hbar}{4} \lim_{\mathbf{k} \rightarrow \mathbf{k}_1^*} \bar{k}_y \frac{\partial \hat{u}(\mathbf{k})^*}{\partial k_x} \\ &= \frac{\sqrt{3}\hbar}{8} \lim_{k_y \rightarrow 4\pi\sqrt{3}/9a} \frac{\sin(\sqrt{3}k_y a/2) + \sin(\sqrt{3}k_y a)}{1 + 2 \cos(\sqrt{3}k_y a/2)} \\ &= \frac{3\hbar}{16} = 0.1875\hbar, \end{aligned} \quad (28)$$

which uses $\bar{k}_y a = (\sin(\sqrt{3}k_y a/2) + \sin(\sqrt{3}k_y a)) / \sqrt{3}$. Notice that it is essential to use the periodic function \bar{k}_y in the OAM operator $\hat{l}_{z\mathbf{k}}$ and in Eq. (28) to produce a finite result for $\mathcal{L}_{zn}(\mathbf{k}_1^*)$.

Suppose wavevector $\mathbf{k}' = \underline{R}_z(\theta) \cdot \mathbf{k}$ is obtained from wavevector \mathbf{k} by applying the rotation operator

$$\underline{R}_z(\theta) = \begin{pmatrix} \cos \theta & \sin \theta \\ -\sin \theta & \cos \theta \end{pmatrix} \quad (29)$$

about the z axis. For $\theta = \pi/3$, it is easy to show that $\Gamma_{\mathbf{k}'} = \Gamma_{\mathbf{k}} = \Gamma_{-\mathbf{k}}$ and, using Eq. (22), that $\underline{X}^{-1}(\mathbf{k}') = \underline{X}(\mathbf{k})^* = \underline{X}(-\mathbf{k})$. So with high-symmetry points $\mathbf{k}_m^* = \underline{R}_z(\pi/3) \cdot \mathbf{k}_{m-1}^*$ and \mathbf{k}_{m-1}^* rotated with respect to one another by $\pi/3$, $\mathcal{L}_{zn}(\mathbf{k}_m^*) = \mathcal{L}_{zn}(-\mathbf{k}_{m-1}^*) = -\mathcal{L}_{zn}(\mathbf{k}_{m-1}^*)$. Hence, the OAM changes sign around the reciprocal-space hexagon in Fig. 2.

IV. FM HONEYCOMB WITH DM INTERACTION

We next consider the FM honeycomb lattice shown in the inset to Fig. 4 with spins up and DM interaction D between next-nearest neighbors. The Hamiltonian is then given by

$$\begin{aligned} H &= -J \sum_{\langle i,j \rangle} \mathbf{S}_i \cdot \mathbf{S}_j - D \sum_{\langle\langle i,j \rangle\rangle} \mathbf{z} \cdot (\mathbf{S}_i \times \mathbf{S}_j) \\ &\quad + D \sum_{\langle\langle i,j \rangle\rangle} \mathbf{z} \cdot (\mathbf{S}_i \times \mathbf{S}_j) - K \sum_i S_{iz}^2, \end{aligned} \quad (30)$$

where the first DM sum runs over the first triangle shown in the inset to Fig. 4 and the second sum with opposite sign runs over the second triangle. The anisotropy $K > 0$ is assumed to be sufficiently large to prevent the spins from tilting away from the z axis.

We then obtain

$$\underline{L}(\mathbf{k}) = \frac{3JS}{2} \begin{pmatrix} 1 - G_{\mathbf{k}} & -\Gamma_{\mathbf{k}}^* & 0 & 0 \\ -\Gamma_{\mathbf{k}} & 1 + G_{\mathbf{k}} & 0 & 0 \\ 0 & 0 & 1 + G_{\mathbf{k}} & -\Gamma_{\mathbf{k}}^* \\ 0 & 0 & -\Gamma_{\mathbf{k}} & 1 - G_{\mathbf{k}} \end{pmatrix}, \quad (31)$$

where $G_{\mathbf{k}} = d \Theta_{\mathbf{k}}$ with $d = -2D/3J$ and

$$\Theta_{\mathbf{k}} = 4 \cos(3k_x a/2) \sin(\sqrt{3}k_y a/2) - 2 \sin(\sqrt{3}k_y a). \quad (32)$$

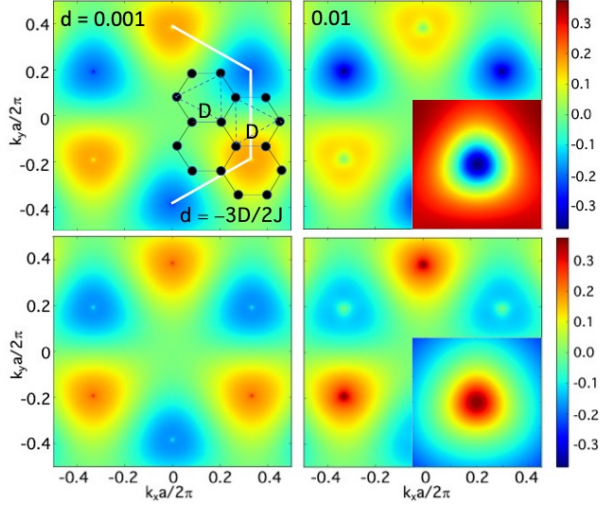


FIG. 4. The OAM of the FM honeycomb lattice with DM interaction $d = -3D/2J$ versus \mathbf{k} . Results for the upper band are shown at the top and for the lower band at the bottom. For $d = 0.01$, insets blow up the regions around \mathbf{k}_1^* with widths $\Delta k_{x,y} = 0.2\pi/a$

Because the anisotropy $\kappa = 2K/3|J|$ merely shifts the magnon energies

$$\hbar\omega_{1,2}(\mathbf{k}) = 3JS \left\{ 1 + \kappa \pm \sqrt{|\Gamma_{\mathbf{k}}|^2 + G_{\mathbf{k}}^2} \right\} \quad (33)$$

but does not affect the OAM, we neglect its contribution to $\underline{L}(\mathbf{k})$.

It follows that

$$\underline{X}^{-1}(\mathbf{k}) = \frac{1}{\sqrt{2}\Gamma_{\mathbf{k}}^*} \begin{pmatrix} -\Gamma_{\mathbf{k}}^* F_{\mathbf{k}}^- & \Gamma_{\mathbf{k}}^* F_{\mathbf{k}}^+ & 0 & 0 \\ |\Gamma_{\mathbf{k}}| F_{\mathbf{k}}^+ & |\Gamma_{\mathbf{k}}| F_{\mathbf{k}}^- & 0 & 0 \\ 0 & 0 & -\Gamma_{\mathbf{k}}^* F_{\mathbf{k}}^- & \Gamma_{\mathbf{k}}^* F_{\mathbf{k}}^+ \\ 0 & 0 & |\Gamma_{\mathbf{k}}| F_{\mathbf{k}}^+ & |\Gamma_{\mathbf{k}}| F_{\mathbf{k}}^- \end{pmatrix}, \quad (34)$$

where

$$F_{\mathbf{k}}^{\pm} = 1 \pm \frac{G_{\mathbf{k}}}{\sqrt{|\Gamma_{\mathbf{k}}|^2 + G_{\mathbf{k}}^2}}. \quad (35)$$

Since $F_{\mathbf{k}}^{\pm}$ is real, it is simple to show that

$$\mathcal{L}_{z1}(\mathbf{k}) = \frac{\hbar}{4} F_{\mathbf{k}}^+ \frac{\Gamma_{\mathbf{k}}}{|\Gamma_{\mathbf{k}}|} \hat{l}_{z\mathbf{k}} \frac{\Gamma_{\mathbf{k}}^*}{|\Gamma_{\mathbf{k}}|}, \quad (36)$$

$$\mathcal{L}_{z2}(\mathbf{k}) = \frac{\hbar}{4} F_{\mathbf{k}}^- \frac{\Gamma_{\mathbf{k}}}{|\Gamma_{\mathbf{k}}|} \hat{l}_{z\mathbf{k}} \frac{\Gamma_{\mathbf{k}}^*}{|\Gamma_{\mathbf{k}}|} \quad (37)$$

for the lower and upper magnon bands, respectively. Because $G_{-\mathbf{k}} = -G_{\mathbf{k}}$ and $F_{-\mathbf{k}}^{\pm} = F_{\mathbf{k}}^{\mp}$, the OAM satisfies the relation $\mathcal{L}_{z1}(\mathbf{k}) = -\mathcal{L}_{z2}(-\mathbf{k})$ and is no longer an odd function of \mathbf{k} within a single band.

Numerical results for the OAM at $d = 0.001$ and 0.01 are plotted in Fig. 4. While the OAM for the lower band

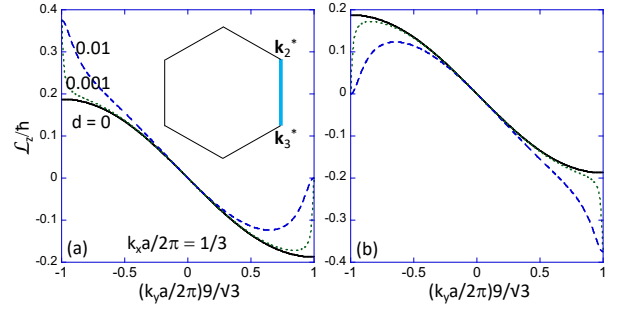


FIG. 5. The OAM of the FM honeycomb lattice along the vertical edge of the BZ with $k_x a/2\pi = 1/3$ from $k_y a/2\pi = -\sqrt{3}/9$ to $\sqrt{3}/9$ with $d = 0, 0.001$, and 0.01 . Results for the lower and upper bands are shown in (a) and (b), respectively.

on the bottom of Fig. 4 is biased towards positive values, the OAM for the upper band on the top is biased towards negative values. Nevertheless, the sum of the OAM over the two bands vanishes, as guaranteed by the symmetry relation above.

These results are verified by the one-dimensional slice along the edge of the BZ plotted in Fig. 5 with $k_x a/2\pi = 1/3$ and $k_y a/2\pi$ running from $-\sqrt{3}/9$ to $\sqrt{3}/9$. The corners \mathbf{k}_3^* and \mathbf{k}_2^* of the BZ lie at the beginning and end of this path. For $d = 0$, the OAM equals $\pm 0.1875\hbar$ at the corners of the BZ for both bands. But even a small DM interaction changes that result dramatically.

This can be readily seen from an exact solution. Since $\Theta_{\mathbf{k}_{2m}^*} = 3\sqrt{3} > 0$ and $\Theta_{\mathbf{k}_{2m+1}^*} = -3\sqrt{3} < 0$, it follows that $F_{\mathbf{k}_{2m}^*}^+ = 2$, $F_{\mathbf{k}_{2m+1}^*}^+ = 0$, $F_{\mathbf{k}_{2m}^*}^- = 0$, and $F_{\mathbf{k}_{2m+1}^*}^- = 2$. Using the results of the previous section, we then find that for $d \neq 0$,

$$\mathcal{L}_{z1}(\mathbf{k}_{2m}^*) = \frac{3\hbar}{8} = 0.375\hbar, \quad (38)$$

$$\mathcal{L}_{z1}(\mathbf{k}_{2m+1}^*) = 0, \quad (39)$$

$$\mathcal{L}_{z2}(\mathbf{k}_{2m}^*) = 0, \quad (40)$$

$$\mathcal{L}_{z2}(\mathbf{k}_{2m+1}^*) = -\frac{3\hbar}{8} = -0.375\hbar, \quad (41)$$

in agreement with the numerical results of Fig. 5. Remarkably, these exact results are satisfied in the presence of infinitesimal values of the DM interaction. But as can be easily seen from Figs. 4 and 5, the region around \mathbf{k}^* with a large or vanishingly small value of $\mathcal{L}_{zn}(\mathbf{k})$ shrinks as $d \rightarrow 0$. Notice that Figs. 5(a) and (b) satisfy the symmetry relation $\mathcal{L}_{z1}(\mathbf{k}) = -\mathcal{L}_{z2}(-\mathbf{k})$.

V. AF HONEYCOMB

Finally, we consider the AF honeycomb lattice in Fig. 6(a) with alternating up and down spins, exchange coupling $J < 0$, easy-axis anisotropy K , and DM inter-

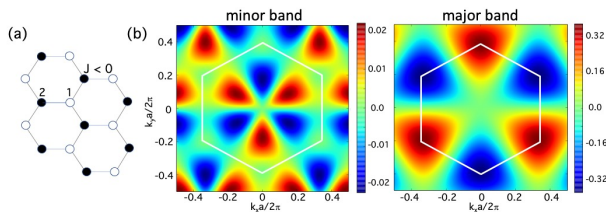


FIG. 6. (a) A honeycomb lattice with AF exchange $J < 0$ between up (closed circles, site 2) and down (open circles, site 1) spins. (b) The OAM of the minor (left) and major (right) bands versus \mathbf{k} for $\kappa = 0$.

action D . Then

$$\underline{L}(\mathbf{k}) = -\frac{3JS}{2} \begin{pmatrix} 1 + \kappa & 0 & 0 & -\Gamma_{\mathbf{k}}^* \\ 0 & 1 + \kappa & -\Gamma_{\mathbf{k}} & 0 \\ 0 & -\Gamma_{\mathbf{k}}^* & 1 + \kappa & 0 \\ -\Gamma_{\mathbf{k}} & 0 & 0 & 1 + \kappa \end{pmatrix} \quad (42)$$

with corresponding

$$\underline{X}^{-1}(\mathbf{k}) = \frac{1}{\sqrt{2f_{\mathbf{k}}\Gamma_{\mathbf{k}}^*}} \begin{pmatrix} -h_{\mathbf{k}}^+\Gamma_{\mathbf{k}}^* & 0 & 0 & h_{\mathbf{k}}^-\Gamma_{\mathbf{k}}^* \\ 0 & h_{\mathbf{k}}^-g_{\mathbf{k}}^+ & -h_{\mathbf{k}}^+g_{\mathbf{k}}^- & 0 \\ 0 & h_{\mathbf{k}}^-\Gamma_{\mathbf{k}}^* & -h_{\mathbf{k}}^+\Gamma_{\mathbf{k}}^* & 0 \\ -h_{\mathbf{k}}^+g_{\mathbf{k}}^- & 0 & 0 & h_{\mathbf{k}}^-g_{\mathbf{k}}^+ \end{pmatrix}, \quad (43)$$

where $f_{\mathbf{k}} = \sqrt{(1 + \kappa)^2 - |\Gamma_{\mathbf{k}}|^2}$, $g_{\mathbf{k}}^{\pm} = 1 + \kappa \pm f_{\mathbf{k}}$, and $h_{\mathbf{k}}^{\pm} = \sqrt{g_{\mathbf{k}}^{\pm}}$.

Because the DM interactions shift the degenerate mode frequencies

$$\omega_{1,2}(\mathbf{k}) = 3|J|S \left\{ \sqrt{(1 + \kappa)^2 - |\Gamma_{\mathbf{k}}|^2} + G_{\mathbf{k}} \right\} \quad (44)$$

through the $G(\mathbf{k})$ term but do not affect the OAM, we neglect their contribution to $\underline{L}(\mathbf{k})$ above. Surprisingly, the degenerate magnon bands exhibit distinct OAM with

$$\mathcal{L}_{z1}(\mathbf{k}) = \frac{\hbar}{4} \frac{1 + \kappa + f_{\mathbf{k}}}{f_{\mathbf{k}}} \frac{\Gamma_{\mathbf{k}}}{|\Gamma_{\mathbf{k}}|} \hat{l}_{z\mathbf{k}} \frac{\Gamma_{\mathbf{k}}^*}{|\Gamma_{\mathbf{k}}|}, \quad (45)$$

$$\mathcal{L}_{z2}(\mathbf{k}) = -\frac{\hbar}{4} \frac{1 + \kappa - f_{\mathbf{k}}}{f_{\mathbf{k}}} \frac{\Gamma_{\mathbf{k}}}{|\Gamma_{\mathbf{k}}|} \hat{l}_{z\mathbf{k}} \frac{\Gamma_{\mathbf{k}}^*}{|\Gamma_{\mathbf{k}}|}. \quad (46)$$

As seen in Fig. 6(b), the major ($n = 1$) and minor ($n = 2$) bands have different OAM patterns but are both threefold symmetric. Notice that $\mathcal{L}_{\text{av}}(\mathbf{k}) = (\mathcal{L}_{z1}(\mathbf{k}) + \mathcal{L}_{z2}(\mathbf{k}))/2$ for the two bands of the AF honeycomb lattice equals the OAM $\mathcal{L}_{zn}(\mathbf{k})$ of the FM honeycomb lattice with $D = 0$, given by Eq. (23) and plotted in Fig. 3(b).

At the BZ corners \mathbf{k}^* , $\Gamma_{\mathbf{k}^*} = 0$, $f_{\mathbf{k}^*} = 1$, and the magnon frequencies reach maxima of $\omega_n(\mathbf{k}^*) = 3|J|S(1 + \kappa \pm 3\sqrt{3}d)$ at \mathbf{k}_{2m}^* and \mathbf{k}_{2m+1}^* , respectively. Comparing Eqs. (45) and (46) with Eq. (23), we find that $\mathcal{L}_{z1}(\mathbf{k}^*) = \pm(3\hbar/8)(1 + \kappa/2)$ and $\mathcal{L}_{z2}(\mathbf{k}^*) = \mp(3\hbar/16)\kappa$. Hence, the average amplitude $|\mathcal{L}_{\text{av}}(\mathbf{k}^*)|$ of the two bands of the AF honeycomb lattice equals $3\hbar/16$, as expected.

VI. CONCLUSION

The theory developed in this paper can be easily extended to treat many real three-dimensional materials that contain honeycomb lattices lying within their ab planes. Sivadas *et al.* [26] reviewed the the magnetic phase diagrams of honeycomb systems with chemical formula ABX_3 . Some examples of FM honeycomb lattices within that class are CrSiTe_3 and CrGeTe_3 [27–29]. Two other Cr-based FM honeycomb systems are CrI_3 [30, 31] and CrCl_3 [32]. Two examples of AF honeycomb lattices are MnPS_3 and MnPSe_3 [33].

The exact calculations in this paper reveal several pertinent points about the OAM of magnons on honeycomb lattices. First, finite results for the OAM at high-symmetry points \mathbf{k}^* are only reached if periodic functions \bar{k}_x and \bar{k}_y are used in the OAM operator $\hat{l}_{z\mathbf{k}}$. If non-periodic terms k_x and k_y were retained in the OAM operator, then the OAM would diverge at the high-symmetry points \mathbf{k}^* . Second, the OAM of the FM and AF honeycomb lattices are closely connected. The average OAM of the major and minor AF honeycomb bands equals the OAM of the FM bands. Third, the largest OAM for the pure honeycomb lattice with amplitude $3\hbar/8$ is still substantially less than \hbar . So the spin angular momentum of a single spin flip is bigger than the largest OAM. Fourth, the DM interaction produced by SO coupling controls the behavior of the OAM near the corners of the BZ, no matter how small the size of d . We conclude that once the network of exchange interactions generates an OAM by confining the magnons, SO coupling can still have important effects. Experimentally, the maximum OAM expected for a FM honeycomb material with even a small to moderate value of the DM interaction should be about $0.375\hbar$.

Although performed at zero temperature, these calculations indicate the available magnon states that can be filled at nonzero temperatures. For the FM honeycomb lattice with $D = 0$, the symmetry relation $\mathcal{L}_{zn}(\mathbf{k}) = -\mathcal{L}_{zn}(-\mathbf{k})$ for magnon bands $n = 1$ and 2 implies that the thermal average $\langle \mathcal{L}_z \rangle$ vanishes due to the integral over wavevectors \mathbf{k} . As discussed above, the DM interaction D breaks that symmetry relation leaving only $\mathcal{L}_{z1}(\mathbf{k}) = -\mathcal{L}_{z2}(-\mathbf{k})$. Consequently, the lower or upper magnon band will carry positive or negative OAM, respectively. This implies that $\langle \mathcal{L}_z \rangle$ peaks at a temperature T of order D^2/J . We will examine this behavior more carefully in future work.

Even for the simple case of a honeycomb lattice with a single exchange interaction, nearest-neighbor DM interactions, and easy-axis anisotropy, many questions remain unanswered. What is the coupling between the spin and orbital angular momentum: do they tend to lie parallel or antiparallel? What is the effect of next-neighbor exchange couplings for both FM and AF honeycomb lattices? Of magnetic fields? Is there some easy way to understand the qualitative difference between the OAM of the major and minor bands of the AF honeycomb lat-

tice? Since the major and minor bands lie at the same energy and momentum, can OAM be easily exchanged between the magnons of the two bands? We hope that future research on the OAM of magnons in other non-Bravais lattices will be motivated by the exact results presented in this work.

We thank Jason Gardner for useful conversations. Research sponsored by the U.S. Department of Energy, Office of Basic Energy Sciences, Materials Sciences and Engineering Division. The data that support the findings of this study are available from the corresponding author upon reasonable request.

-
- [1] A. Einstein and W.J. de Hass. Experimental proof of the existence of ampere's molecular currents. *Proc. KNAW*, 18:696, 1915.
- [2] S. J. Barnett. Magnetization by rotation. *Phys. Rev.*, 6:239–270, Oct 1915.
- [3] Ryo Matsumoto and Shuichi Murakami. Theoretical prediction of a rotating magnon wave packet in ferromagnets. *Phys. Rev. Lett.*, 106:197202, May 2011.
- [4] Ryo Matsumoto and Shuichi Murakami. Rotational motion of magnons and the thermal hall effect. *Phys. Rev. B*, 84:184406, Nov 2011.
- [5] Robin R. Neumann, Alexander Mook, Jürgen Henk, and Ingrid Mertig. Orbital magnetic moment of magnons. *Phys. Rev. Lett.*, 125:117209, Sep 2020.
- [6] Simon Streib. Difference between angular momentum and pseudoangular momentum. *Phys. Rev. B*, 103:L100409, Mar 2021.
- [7] V. M. Tsukernik. Some Features of the Gyromagnetic Effect in Ferrodielectrics at Low Temperatures. *Soviet Journal of Experimental and Theoretical Physics*, 50:1631, June 1966.
- [8] V. S. Garmatyuk and V. M. Tsukernik. The Gyromagnetic Effect in an Antiferromagnet at Low Temperatures. *Soviet Journal of Experimental and Theoretical Physics*, 26:1035, May 1968.
- [9] Alexy D. Karenowska, A. V. Chumak, A. A. Serga, and Burkard Hillebrands. *Magnon Spintronics*, pages 1–38. Springer Netherlands, Dordrecht, 2014.
- [10] Satoshi Fujimoto. Hall effect of spin waves in frustrated magnets. *Phys. Rev. Lett.*, 103:047203, Jul 2009.
- [11] Hosho Katsura, Naoto Nagaosa, and Patrick A. Lee. Theory of the thermal hall effect in quantum magnets. *Phys. Rev. Lett.*, 104:066403, Feb 2010.
- [12] Y. Onose, T. Ideue, H. Katsura, Y. Shiomi, N. Nagaosa, and Y. Tokura. Observation of the magnon hall effect. *Science*, 329(5989):297–299, 2010.
- [13] Ran Cheng, Satoshi Okamoto, and Di Xiao. Spin Nernst effect of magnons in collinear antiferromagnets. *Phys. Rev. Lett.*, 117:217202, Nov 2016.
- [14] L. Marrucci, C. Manzo, and D. Paparo. Optical spin-to-orbital angular momentum conversion in inhomogeneous anisotropic media. *Phys. Rev. Lett.*, 96:163905, Apr 2006.
- [15] Lifa Zhang and Qian Niu. Angular momentum of phonons and the Einstein–de Haas effect. *Phys. Rev. Lett.*, 112:085503, Feb 2014.
- [16] Masato Hamada, Emi Minamitani, Motoaki Hirayama, and Shuichi Murakami. Phonon angular momentum induced by the temperature gradient. *Phys. Rev. Lett.*, 121:175301, Oct 2018.
- [17] Randy S. Fishman, Jason Gardner, and Satoshi Okamoto, <http://arXiv.org/abs/2203.15677> (2022).
- [18] J. A. Haigh, A. Nunnenkamp, A. J. Ramsay, and A. J. Ferguson. Triple-resonant brillouin light scattering in magneto-optical cavities. *Phys. Rev. Lett.*, 117:133602, Sep 2016.
- [19] Sanchar Sharma, Yaroslav M. Blanter, and Gerrit E. W. Bauer. Light scattering by magnons in whispering gallery mode cavities. *Phys. Rev. B*, 96:094412, Sep 2017.
- [20] A. Osada, A. Gloppe, Y. Nakamura, and K. Usami. Orbital angular momentum conservation in brillouin light scattering within a ferromagnetic sphere. *New Journal of Physics*, 20(10):103018, oct 2018.
- [21] Yuanyuan Jiang, H. Y. Yuan, Z.-X. Li, Zhenyu Wang, H. W. Zhang, Yunshan Cao, and Peng Yan. Twisted magnon as a magnetic tweezer. *Phys. Rev. Lett.*, 124:217204, May 2020.
- [22] Seungho Lee and Se Kwon Kim. Generation of magnon orbital angular momentum by a skyrmion-textured domain wall in a ferromagnetic nanotube. *Frontiers in Physics*, 10, 2022.
- [23] E. O. Kamenetskii. Magnetic dipolar modes in magnon-polariton condensates. *Journal of Modern Optics*, 68(21):1147–1172, 2021.
- [24] L.D. Landau and E.M. Lifshitz. *The Classical Theory of Fields*. Butterworth-Heinemann, Fourth revised english edition, 1973.
- [25] Randy S. Fishman, Jaime Fernandez-Baca, and Toomas Rõõm. *Spin-Wave Theory and its Applications to Neutron Scattering and THz Spectroscopy*. Morgan and Claypool Publishers, San Rafael, 2018.
- [26] Nikhil Sivadas, Matthew W. Daniels, Robert H. Swendsen, Satoshi Okamoto, and Di Xiao. Magnetic ground state of semiconducting transition-metal trichalcogenide monolayers. *Phys. Rev. B*, 91:235425, Jun 2015.
- [27] V. Carreaux, F. Moussa, and M. Spiesser. 2d ising-like ferromagnetic behaviour for the lamellar CrSi₂Te₆ compound: A neutron scattering investigation. *Europhysics Letters (EPL)*, 29(3):251–256, jan 1995.
- [28] V. Carreaux, D. Brunet, G. Ouvrard, and G. Andre. Crystallographic, magnetic and electronic structures of a new layered ferromagnetic compound Cr₂Ge₂Te₆. *Journal of Physics Condensed Matter*, 7(1):69–87, January 1995.
- [29] L. D. Casto, A. J. Clune, M. O. Yokosuk, J. L. Musfeldt, T. J. Williams, H. L. Zhuang, M.-W. Lin, K. Xiao, R. G. Hennig, B. C. Sales, J.-Q. Yan, and D. Mandrus. Strong spin-lattice coupling in CrSiTe₃. *APL Materials*, 3(4):041515, 2015.
- [30] Michael A. McGuire, Hemant Dixit, Valentino R. Cooper, and Brian C. Sales. Coupling of crystal structure and magnetism in the layered, ferromagnetic insulator CrI₃. *Chemistry of Materials*, 27(2):612–620, 2015.
- [31] Lebing Chen, Jae-Ho Chung, Bin Gao, Tong Chen, Matthew B. Stone, Alexander I. Kolesnikov, Qingzhen Huang, and Pengcheng Dai. Topological spin excitations in honeycomb ferromagnet CrI₃. *Phys. Rev. X*, 8:041028,

Nov 2018.

- [32] X. Li, S. Do, J. Yan, M. McGuire, G. Granroth, S. Mu, T. Berlijn, V. Cooper, A. Christianson, and L. Lindsay, Phonons and phase symmetries in bulk CrCl_3 from scattering measurements and theory, arXiv/2209.02394.
- [33] A. R. Wildes, B. Roessli, B. Lebech, and K. W. Godfrey. Spin waves and the critical behaviour of the magnetization in MnPS_3 . *J. Phys.: Condens. Matter*, 10:6417, 1998.